IEEE Access
Multidisciplinary | Rapid Review | Open Access Journal

Received May 15, 2021, accepted May 25, 2021, date of publication May 28, 2021, date of current version June 8, 2021.

*Digital Object Identifier 10.1109/ACCESS.2021.3084736*

# Wideband Circularly Polarized Antenna With Reconfigurable 2-Dimensional Axial Ratio Beamwidth

**JEONG-WOOK KIM[1], JU-IK OH[1], SANG HYUCK HAN[1], WON-YOUNG SONG[2], SOO-CHANG CHAE[1], AND JONG-WON YU[1] (Member, IEEE)**

[1]School of Electrical Engineering, Korea Advanced Insititute of Science and Technology (KAIST), Daejeon 34141, Republic of Korea
[2]Electronics and Telecommunications Research Institute (ETRI), Daejeon 34129, Republic of Korea

Corresponding author: Soo-Chang Chae (wintbud@kaist.ac.kr)

This work was supported in part by the Ministry of Science and ICT (MSIT), South Korea, under the Information Technology Research Center (ITRC) Support Program Supervised by the Institute of Information and Communications Technology Planning and Evaluation (IITP) under Grant IITP-2021-0-01778.

**ABSTRACT** This paper proposes a wideband circularly polarized antenna with a reconfigurable 2-dimensional axial ratio. For mobile satellite communication, the low profile CP antenna with wide axial ratio scanning and a wide frequency bandwidth is essential. In this paper, we propose the wideband CP antenna with an axial ratio controller. The axial ratio deteriorates when the difference between transverse modes (TM)01 and TM10 gets larger. Therefore, in the proposed antenna, the axial ratio controller is used to compensate for the difference by controlling the amplitude and phase of the received signals. The proposed antenna has three mode states for the 2-dimensional axial ratio region. In a simulation of the wideband CP antenna, the axial ratio was below 3 dB in the 2-dimensional scanning region from $-60°$ to $60°$ at every azimuth angle in the 20% factional frequency bandwidth. To verify the proposed antenna with the axial ratio controller, the wideband CP antenna is implemented at 5.8 GHz. A low noise amplifier (LNA) and digital phase shifters are employed for the axial ratio controller. The measured axial ratio was below 3 dB in the 2-dimensional scanning region from $-60°$ to $60°$ at every azimuth angle in the 20% factional frequency bandwidth.

**INDEX TERMS** Wide-angle axial ratio beamwidth, wide band axial ratio, amplitude and phase control, 2-dimensional reconfigurable axial ratio.

## I. INTRODUCTION

The circularly polarized (CP) antenna has been used in various applications to address issues with mobility, weather penetration, and to reduce multipath reflections. Various papers have proposed novel CP antennas to improve axial ratio bandwidth, CP gain, and polarization reconfigurable performance [1]–[9]. The L-probe feeding patch antenna with a novel radiator was presented for dual operating bandwidth [1]. By designing the proper gap between the L-probe feeder and patch antenna, the amplitude and phase of the electrical field are controlled to form circular polarization in a dual-band. A high gain dual CP antenna using 3D printing technology was designed in [2]. It employs a high order mode cavity for high gain and reducing loss. Orthogonal feeders were used for dual CP performance. The paper in [3] presented a folded dipole, metal column, ME dipole for wide beam and wide band CP performance. For dual CP, the antenna used a the hybrid coupler at a feeder. CP reconfigurable antennas have also been researched [4]–[9]. The CP antennas presented in [4]–[8] employed diode switches for reconfigurable circular polarizations. As a result, they can radiate RHCP (Right Handed Circular Polarization) and LHCP (Left Handed Circular Polarization) by controlling the on and off of diode switch. The CP antenna in [9] used a phase shifter and truncated square metal patch to reconfigure the circular polarization and linear polarization.

The CP antenna is also employed for satellite communication [10]–[12]. Wide axial ratio beamwidth is especially essential for mobile satellite communication for automobile

The associate editor coordinating the review of this manuscript and approving it for publication was Davide Comite.

and unmanned aircraft vehicles (UAVs) due to the variety of angles of the arriving receiving signal. Conventional CP antennas [1]–[9] are not suitable because the reported CP antennas rarely have wide axial ratio beamwidth. Also, when the wide frequency bandwidth of the satellite communication is employed, a wideband CP antenna with wide axial ratio beamwidth is required [13]. For wide axial ratio performance, some researchers have proposed low profile CP antennas [14]–[20]. In [14], a single fed CP antenna with stepped arc-shaped arms was presented. Each arm is split up into two horizontal arc-shaped parts and one vertical part, broadening the axial ratio beamwidth. In [15], a single patch antenna with shorting pins was proposed. The position and radius of these pins change the amplitude of the dual-polarization, leading to widening of the axial ratio beamwidth. However, these antennas have narrow axial ratio bandwidth. In [16], [17], dual-band CP antennas were investigated. A compact CP antenna with an annular metal strip loaded ground plane was employed for wide axial ratio beamwidth [16]. The annular metal strips served as parasitic radiators on the ground and improved the axial ratio beamwidth. Also, a stacked patch antenna with a back modified metallic cavity was studied for wide axial ratio beamwidth in [17]. The height and radius of the cavity were the control points of the axial ratio beamwidth. An aperture coupled CP antenna with a metasurface antenna was introduced in [18]. The various lengths of the slot controlling the phase of the beam pattern and feeding points resulted in improvement of the axial ratio beamwidth. Four integrated printed dipoles were proposed in [19]. The extra thick substrate and metal cavity were designed for wide beamwidth and axial ratio beamwidth. The bandwidth of the CP antenna was also wide. In [20], a wideband CP antenna with two curved arms shaped like an inverted 's' was reported. The distance between the radiator and ground plane of the CP antenna affected the axial ratio beamwidth. However, these CP antennas have a narrow bandwidth with a wide-angle axial ratio [14]–[18]. Also, the 2-dimensional axial ratio region was rarely studied in [15]–[19]. In particular, the height of the antenna in [20] is too high for a low profile antenna application.

Generally, as the beamwidth and bandwidth become wider, the axial ratio becomes worse. The degradation of the axial ratio results from the amplitude and phase difference between TM10 and TM01. In particular, with wideband frequency bandwidth and in the 2-dimensional region, the amplitude and phase difference are hard to maintain properly. The degradation of the axial ratio causes polarization mismatching loss [21]. In this paper, we propose a wideband circularly polarized antenna with a reconfigurable 2-dimensional axial ratio, as shown in Fig. 1. The antenna is designed as a stacked patch antenna for wide bandwidth and operates at 5.2 GHz to 6.4 GHz, with a fractional bandwidth of 20 %. Using a controller, the amplitude of the received signal is controlled by the gain of the low noise amplifier (LNA), and the phase of the received signal is controlled by the digital phase shifter to compensate the difference between TM10 and TM01.

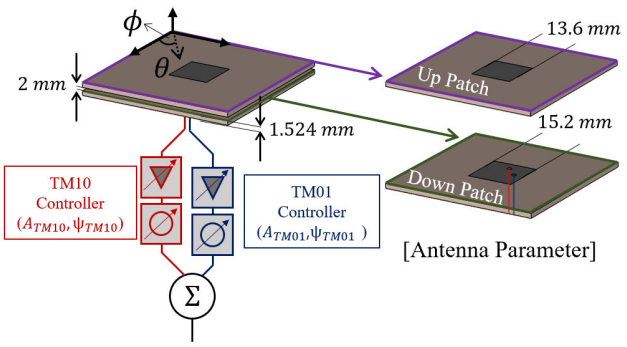


**FIGURE 1.** Proposed antenna structure.

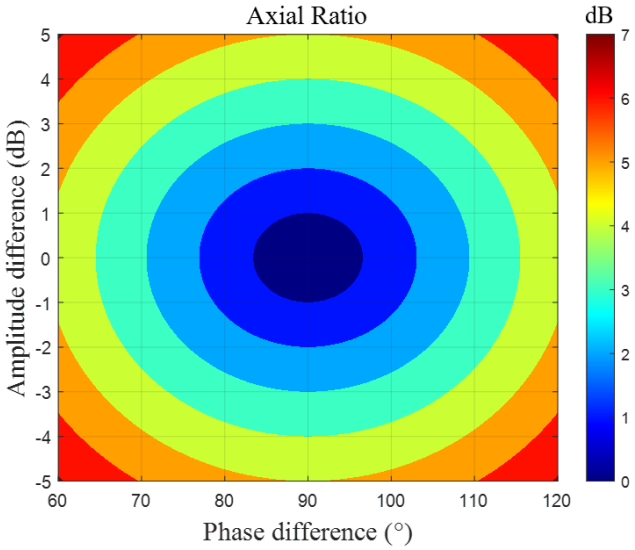


**FIGURE 2.** Axial ratio distribution.

The controller can produce a three-mode state for a 2-dimensional axial ratio region in the wide frequency bandwidth. In conclusion, the axial ratio can be controlled under 3 dB in every frequency band and with a region of elevation angle from −60° to 60° in every azimuth angle. The proposed antenna with the axial ratio controller was implemented for validation. The measured axial ratio in the 2-dimensional region was under 3 dB in 20 % fractional frequency bandwidth.

## II. ANTENNA DESIGN

### A. THEORETICAL ANALYSIS

The axial ratio of a received dual polarized signal is expressed as follows:

$$AR = \sqrt{\frac{1+\alpha^2+\sqrt{(\alpha^4+2\alpha^2 cos(2\Delta\Phi)+1)}}{1+\alpha^2-\sqrt{(\alpha^4+2\alpha^2 cos(2\Delta\Phi)+1)}}} \quad (1)$$

$$\alpha = \frac{E_{TM10}}{E_{TM01}} \quad (2)$$

$$\Delta\Phi = \Phi_{TM10} - \Phi_{TM01}, \quad (3)$$

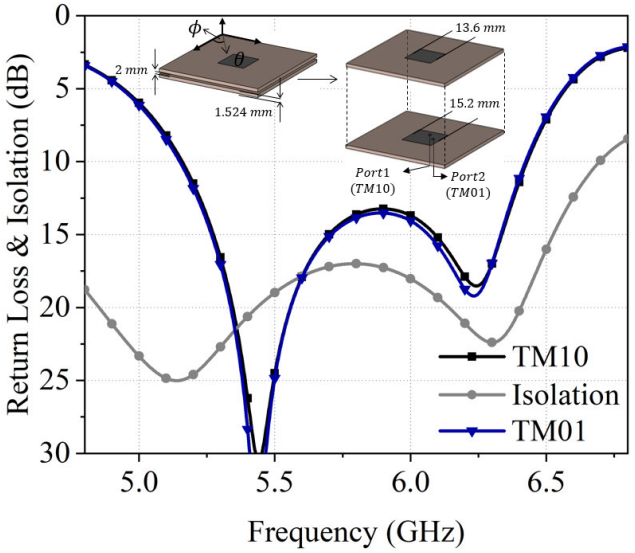


**FIGURE 3.** Simulated return loss and Isolation.

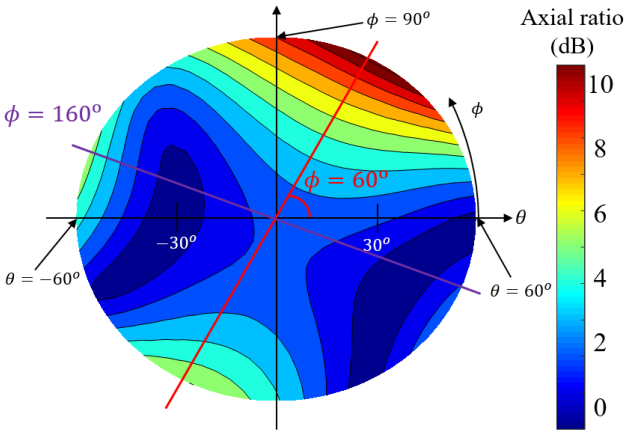


**FIGURE 4.** Axial ratio distribution of original state at 5.8 GHz.

where $E_{TM10}$ and $E_{TM01}$ are the amplitude, and $\Phi_{TM10}$ and $\Phi_{TM01}$ are the phase of the received TM10 signal and TM01 signal respectively, and $\alpha$ is the amplitude difference, and $\Delta\Phi$ is the phase difference between the TM10 and TM01 signals as shown in (2) and (3).

Fig. 2 shows the axial ratio distribution according to the amplitude difference ($\alpha$) and phase difference ($\Delta\Phi$) of the TM10 and TM01 signals. As shown in Fig. 2, the large difference in amplitude and phase makes the axial ratio worse. Under ideal axial ratio conditions, the amplitude difference ($\alpha$) is 0 dB, and the phase difference ($\Delta\Phi$) is 90°, which makes the axial ratio 0 dB. However, in the wide-angle region in the wide frequency bandwidth, the ideal condition is hardly achieved. Therefore, by controlling the gain of the LNA ($A_{TM10}$, $A_{TM01}$) and phase offset of the digital phase shifter ($\Psi_{TM10}$, $\Psi_{TM01}$), the axial ratio can be controlled. The gain in LNA and the phase offset of the phase shifter for the ideal axial ratio are given by,

$$A_{TM10,ctrl} = \begin{cases} A_{LNA} - \alpha & (\alpha > 0) \\ A_{LNA} & (\alpha < 0), \end{cases} \tag{4}$$

$$A_{TM01,ctrl} = \begin{cases} A_{LNA} & (\alpha > 0) \\ A_{LNA} - \alpha & (\alpha < 0), \end{cases} \tag{5}$$

$$\Psi_{TM10,ctrl} = \begin{cases} 180° - \Delta\Phi & (\text{RHCP}) \\ 0 & (\text{LHCP}), \end{cases} \tag{6}$$

$$\Psi_{TM01,ctrl} = \begin{cases} 0 & (\text{RHCP}) \\ 180° - \Delta\Phi & (\text{LHCP}). \end{cases} \tag{7}$$

The gain in LNA ($A_{TM10,ctrl}$, $A_{TM01,ctrl}$) is controlled to compensate the amplitude difference ($\alpha$). When the amplitude difference ($\alpha$) is larger than 0 dB, the ideal gain of the LNA of the TM10 signal ($A_{TM10,ctrl}$) is controlled by a decrease in the amplitude difference ($\alpha$) over the typical gain of LNA ($A_{LNA}$). Then, the gain in the LNA of the TM01 signal ($A_{TM01,ctrl}$) maintains the typical LNA gain ($A_{LNA}$). The phase offset of the digital phase shifter ($\Psi_{TM10,ctrl}$, $\Psi_{TM01,ctrl}$) is also controlled to compensate the phase difference ($\Delta\Phi$). To make the phase difference ($\Delta\Phi$) 90°, the phase offset of 180-$\Delta\Phi$ is selected instead of 90°. Then, the controlled amplitude and phase of the TM10 and TM01 signals are given by

$$E_{TM10,ctrl}e^{j\Phi_{TM10,ctrl}} = A_{TM10,ctrl}e^{j\Psi_{TM10,ctrl}}\left(E_{TM10}(\theta,\phi)e^{j\Phi_{TM10}(\theta,\phi)}\right), \tag{8}$$

$$E_{TM01,ctrl}e^{j\Phi_{TM01,ctrl}} = A_{TM01,ctrl}e^{j\Psi_{TM01,ctrl}}\left(E_{TM01}(\theta,\phi)e^{j\Phi_{TM01}(\theta,\phi)}\right). \tag{9}$$

where $E_{TM10}(\theta,\phi)$ and $E_{TM01}(\theta,\phi)$ are the amplitude, $\Phi_{TM10}(\theta,\phi)$ and $\Phi_{TM01}(\theta,\phi)$ are the phase of the TM10 and TM01 signals, respectively.

Also, the CP beam pattern is as follows:

$$E_{ctrl}(\theta,\phi,\alpha,\Delta\Phi) = \hat{a}_{TM10}E_{TM10,ctrl}e^{j\Phi_{TM10,ctrl}} + \hat{a}_{TM01}E_{TM01,ctrl}e^{j\Phi_{TM01,ctrl}} \tag{10}$$

where $\hat{a}_{TM10}$ and $\hat{a}_{TM01}$ are the unit vector of TM10 signal and TM01 signal, respectively. By controlling LNA gain and phase offset, the controlled amplitude difference ($\alpha_{ctrl}$) becomes 0 dB and the phase difference ($\Delta\Phi_{ctrl}$) changes to 90°. Then, the axial ratio is controlled to be 0 dB.

### *B. SIMULATION RESULTS*

Based on the theoretical analysis, the CP antenna was designed as shown in Fig. 3. Fig. 3 presents the simulation results of the return loss and isolation and the structure of the single antenna. The antenna is a dual-polarized stacked microstrip patch whose operating frequency is from 5.2 GHz to 6.4 GHz. Due to the effect of the stacked patch, the fractional bandwidth is 20 %, which is wider than the typical patch antenna. The antenna has two ports for TM10 and TM01. In its original state, the gain in the LNA of the

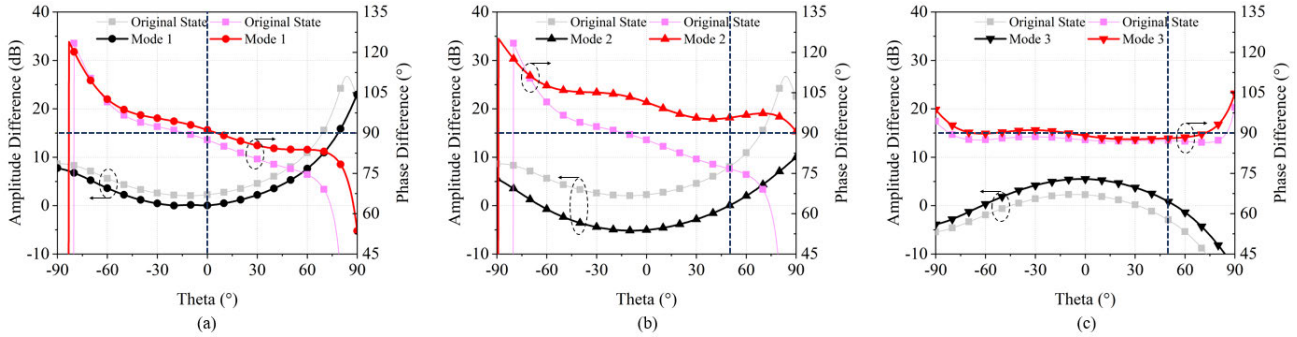


**FIGURE 5.** Amplitude difference and phase difference at 5.8 GHz: (a) $\phi$=60° (b) $\phi$=60° (c) $\phi$=160°.

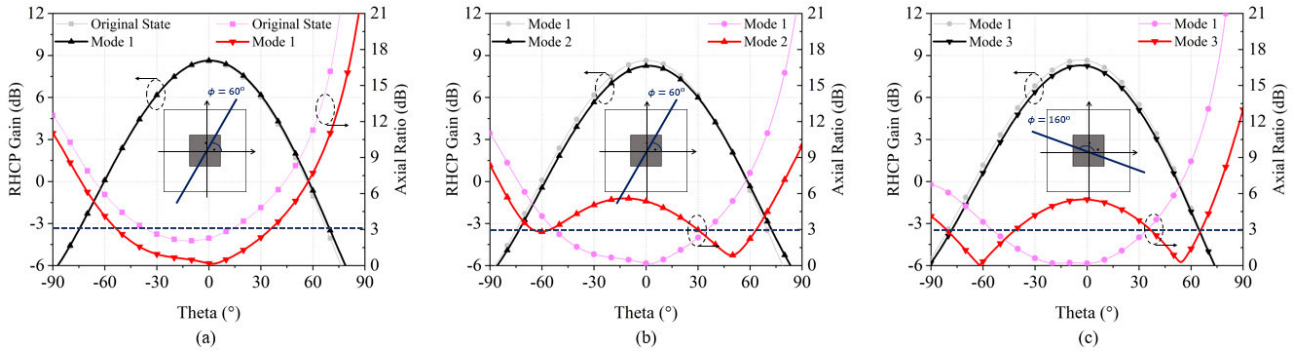


**FIGURE 6.** CP Gain and axial ratio at 5.8 GHz: (a) $\phi$=60° (b) $\phi$=60° (c) $\phi$=160°.

TM10 and TM01 signals is the same ($A_{LNA}$), and the phase offset is 90°. The axial ratio distribution of the antenna in the original state is shown in Fig. 4. The distribution is a 2-dimensional axial ratio value in the region from −60° to 60° of $\theta$ in every azimuth angle. The axial ratio near ($\phi$=0°,$\theta$=30°) and ($\phi$=0°,$\theta$=−30°) is low enough. However, the axial ratio near the center of the antenna is close to 3 dB. Also, the axial ratio degrades as the $\theta$ becomes wider. At a $\phi = 60°$ and $\phi = 160°$, the axial ratio becomes seriously deteriorated as $\theta$ gets wider.

The reason for the degradation of the axial ratio is shown in Fig. 5. In Fig. 5. (a), the amplitude difference ($\alpha$) and phase difference ($\Delta\Phi$) at $\phi = 60°$ are shown according to $\theta$ at 5.8 GHz. The amplitude difference ($\alpha$) increases when $\theta$ becomes wider. The phase difference ($\Delta\Phi$) also becomes bigger than 90° as $\theta$ becomes wider. Therefore, the axial ratio becomes worse. To improve the poor axial ratio region, a reconfigurable mode is proposed to fully control the 2-dimensional axial ratio distribution.

Firstly, the axial ratio near the antenna center is controlled. As shown in Fig. 5(a), the amplitude difference ($\alpha$) and phase difference ($\Delta\Phi$) at the $\theta = 0°$ are 2.24 dB and 87.1°. To make the amplitude difference 0 dB and the phase difference 90°, the gain in the LNA of the TM10 signal ($A_{TM10}$) should be 2.24 dB smaller than the gain of LNA of TM01 signal, and the phase offset of the TM10 signal ($\Psi_{TM10}$) must become 92.9° to compensate the phase difference. Then, the amplitude difference ($\alpha$) and phase difference ($\Delta\Phi$) become 0 dB and 90° at $\theta = 0°$ and that state is mode1. The region with under the 3 dB axial ratio becomes wider than the original state, as shown in Fig. 6 (a). We consider this state to be mode1.

Even in mode1, the wide angle axial ratios at $\phi = 60°$ and $\phi = 160°$ are seriously degraded as shown in Fig. 6 (b) and (c). To control the axial ratio at $\phi = 60°$, a point at $\phi = 60°$, $\theta = 50°$ is selected. In Fig. 5(b), the amplitude difference ($\alpha$) and phase difference ($\Delta\Phi$) at $\phi = 60°$, $\theta = 50°$ are 8 dB and 75.7°. The same control method is used as the first control. This makes the gain of the LNA of the TM10 signal ($A_{TM10}$) 8 dB smaller than that of the TM01 signal and the phase offset of the TM10 ($\Psi_{TM10}$) must become 104.3° to compensate the phase difference. We consider this state to be mode2. The CP gain and axial ratio of mode1 and mode2 are shown in Fig. 6(b). The region ($-50° < \theta < 30°$) can be used as mode1 and other region ($-60° < \theta < -50°$, $30° < \theta < 60°$) can be used as mode2. Then, the axial ratio of all regions is under 3 dB.

Finally, we only have to control the axial ratio at $\phi = 160°$. To control the axial ratio, a point at $\phi = 160°$, $\theta = 50°$ is selected. Using the same method as the first and second control, the axial ratio can be controlled. As shown in Fig. 5(c), the amplitude difference ($\alpha$) and phase difference ($\Delta\Phi$) are close to 0 dB and 90° at $\phi = 160°$, $\theta = 50°$ and the axial ratio is improved as shown in Fig. 6(c). In Fig. 6(c), The region ($-40° < \theta < 32°$) can be used as mode1 and other region ($-60° < \theta < -40°$, $32° < \theta < 60°$) can be used as mode3.

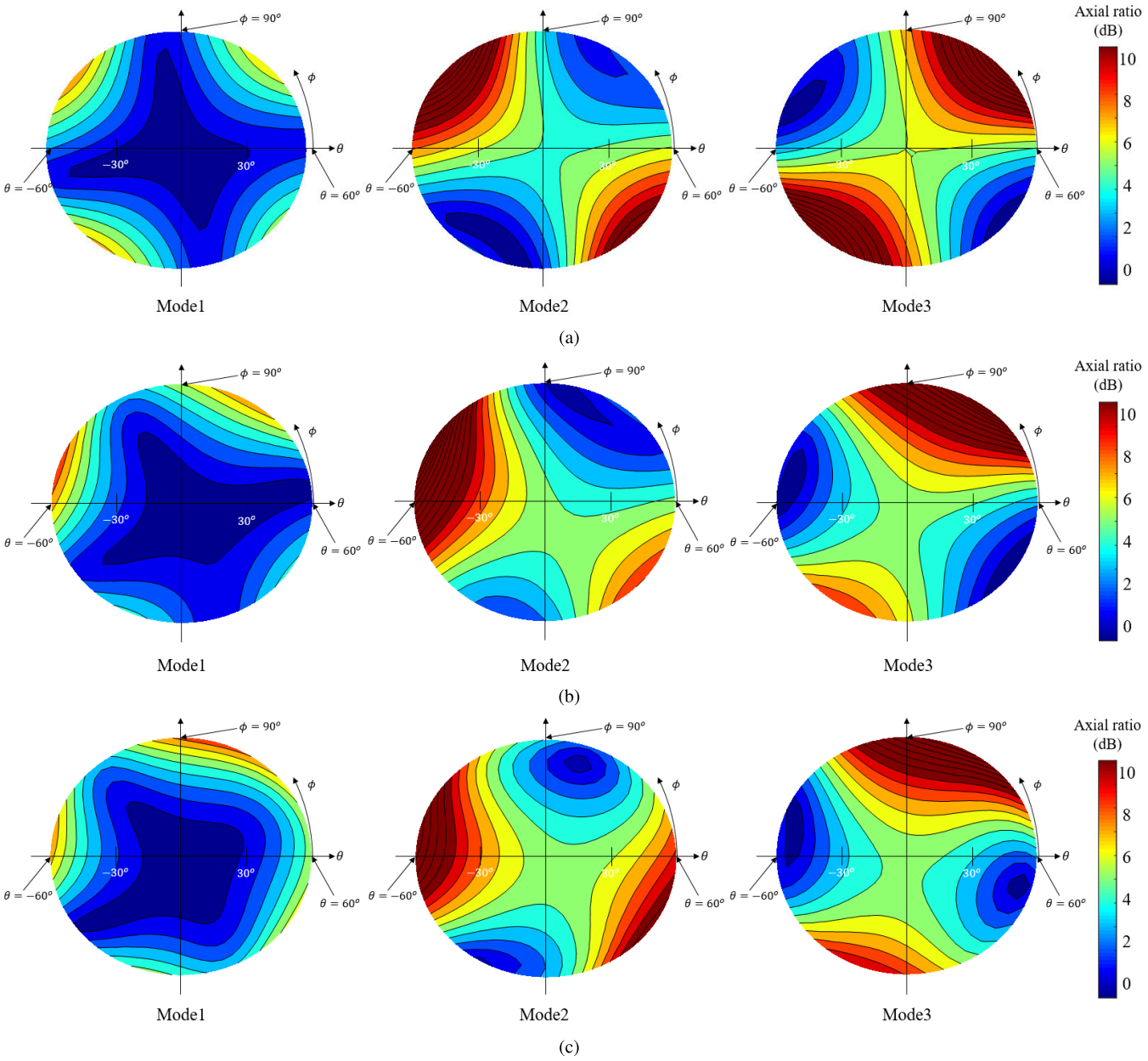


**FIGURE 7.** Axial ratio distribution of mode1, mode2, mode3: (a) 5.2 GHz, (b) 5.8 GHz, (c) 6.4 GHz.

In Fig. 7, the axial ratio distribution of each frequency and region can be observed. As shown in Fig. 7(b), for mode1, the region near the center of the antenna has a low axial ratio level. In the mode2 and mode3 regions the axial ratio is controlled for $\phi = 60°$, $\theta = 50°$ and $\phi = 160°$, $\theta = 50°$. The axial ratio of the region near the control point is improved simultaneously. Also, in Fig. 7(a) and Fig. 7(c), the axial ratio at 5.2 GHz and 6.4 GHz are controlled by the same method used for 5.8 GHz. We note that the axial ratio is controllable in all regions and the frequency band. Furthermore, by reconfiguring mode 1,2 and 3, the axial ratio of all regions can be maintained under 3 dB.

## III. IMPLEMENTATION AND MEASUREMENT

To verify the proposed CP antenna with the reconfigurable 2D axial ratio, the antenna, and the controller were fabricated, as shown in Fig. 8. The dual-polarized stacked patch antenna was implemented in Fig. 8(a). The controller consists of an LNA, 4-bit digital phase shifter, and Wilkinson power divider. The attenuator for LNA can control gain in steps of 0.5 dB, and the phase can be controlled in steps of 22.5°. The controller has 16 channels. Each channel had amplitude and phase errors depending on the phase state. Therefore, we measured the amplitude and phase offset of the RF chains and calibrated them. Before the board calibration, at some phase states, the amplitude errors of the RF chain were over

**TABLE 1. Comparison with the previously reported circularly polarized antennas.**

| Reference | Wide Angle Axial Ratio Bandwidth (%) | Center Freq. (GHz) | 2D Axial ratio ($-60° < \theta < 60°$) | CP Gain in Bandwidth (dB) | Low profile |
|---|---|---|---|---|---|
| [14] (2017) | 0.36 | 2.5 | O | -0.5 | O |
| [15] (2017) | 0.29 | 2.44 | X | 7 | O |
| [16] (2019) | - | Dual Band (1.21, 1.56) | X | 1.98, 4.1 | O |
| [17] (2019) | - | Dual Band (1.23, 1.57) | X | 2.59, 3.4 | O |
| [18] (2019) | 14.6 | 1.51 | X | 7 | O |
| [19] (2018) | 34.5 | 1.45 | X | 3.5 | O |
| [20] (2017) | 40 | 5 | X | 7 | X |
| Proposed | 20 | 5.8 | O | 7 | O |

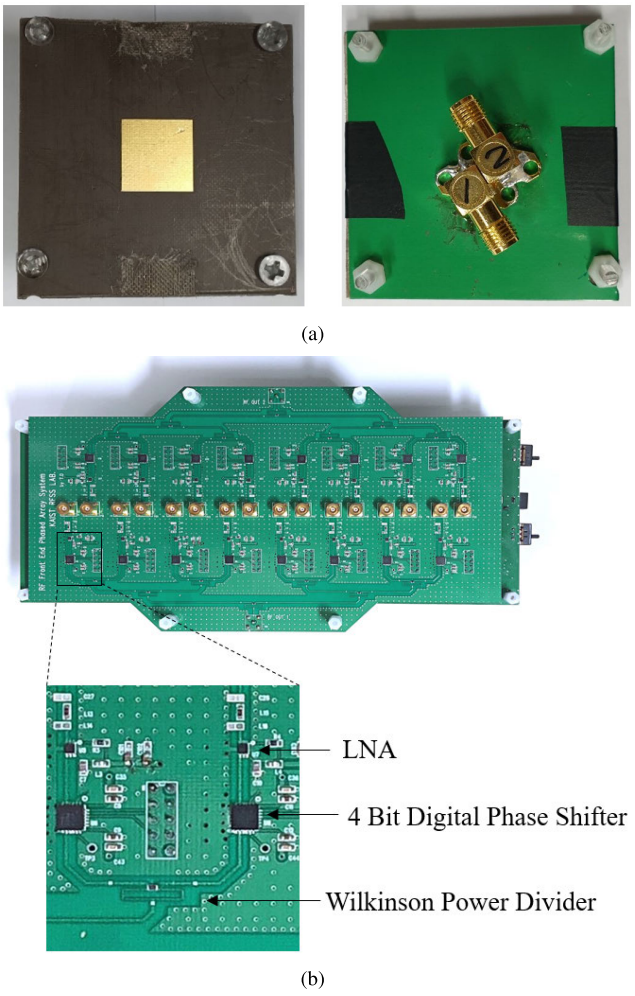


**FIGURE 8. Implemented (a) antenna (b) controller.**

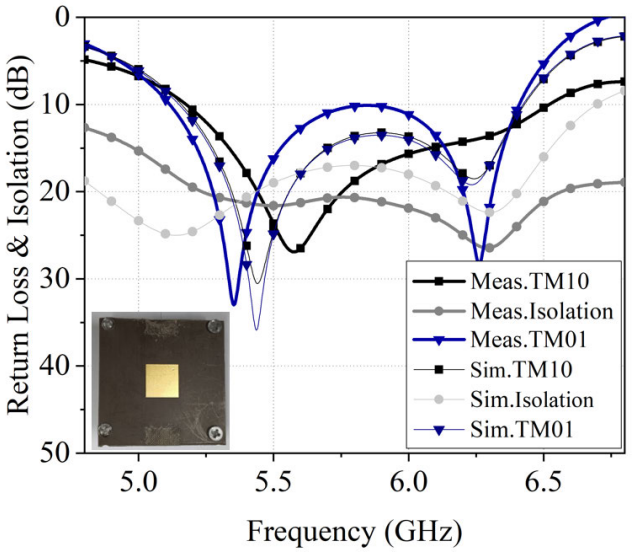


**FIGURE 9. Comparison of simulated and measured return loss and isolation of implemented antenna.**

$\pm 0.5$ dB. After the board amplitude calibration, the amplitude errors were less than $\pm 0.3$ dB. Also, we chose a channel whose phase error was under $\pm 1°$.

Fig. 9 shows a comparison of the simulated and measured return loss and isolation of the antenna. The antenna's measured return loss and isolation were similar to the simulation. The implemented antenna operated from 5.2 GHz to 6.4 GHz. Fig. 10 (a) and (b) show the axial ratio in each mode at 5.2 GHz, Fig. 10(c) and (d) is at 5.8 GHz, and Fig. 10(e) and (f) are the axial ratio at 6.4 GHz. As shown in Fig. 10, in each mode, the axial ratio can be controlled as in the simulation. In the center and edge frequency of the operating frequency bandwidth, the axial ratio was under 3 dB in the region from $-60°$ to $60°$.

Fig. 11 shows the CP radiation pattern at 5.8 GHz in each mode. As the mode changed, the radiation patterns varied. However, the CP gain had only a slight difference. The results of the simulation and measurement showed similar tendencies.

Table 1 summarizes the performance of the proposed antenna and previously reported CP antennas. The meaning of the wide angle ARBW is the frequency bandwidth at which the antenna can maintain under 3 dB axial ratio at elevation angles from $-60°$ to 60 °. Also, 'O' in the 2-dimensional axial ratio indicates whether the antenna can have an axial ratio below 3 dB in the 2-dimensional region, a 360 ° azimuth angle and elevation angle from $-60°$ to $60°$. The CP antennas in [14]–[18] have a narrow bandwidth wide-angle axial ratio. Furthermore, the 2-dimensional axial ratio region was rarely studied in [15]–[19]. In particular, the antenna in [20] is not suitable for low profile antenna applications. On the other hand, the proposed antenna has wide axial ratio bandwidth, and the antenna shows a 2-dimensional low axial ratio

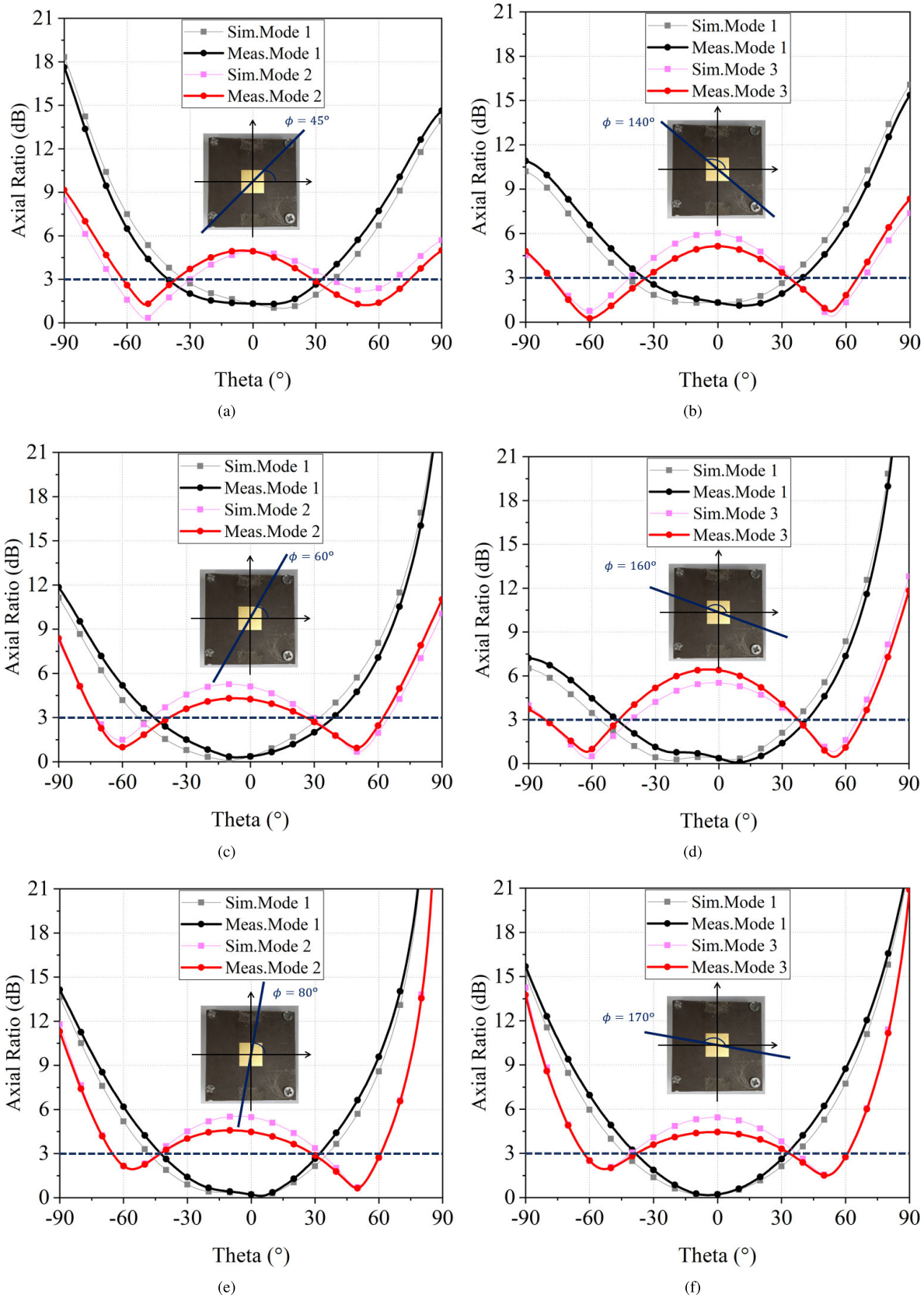


**FIGURE 10.** Measured axial ratio comparison among mode: (a) at 5.2 GHz, $\phi = 45°$ (b) at 5.2 GHz, $\phi = 140°$, (c) at 5.8 GHz, $\phi = 60°$ (d) at 5.8 GHz, $\phi = 160°$ (e) at 6.4 GHz, $\phi = 80°$ (f) at 6.4 GHz, $\phi = 170°$.

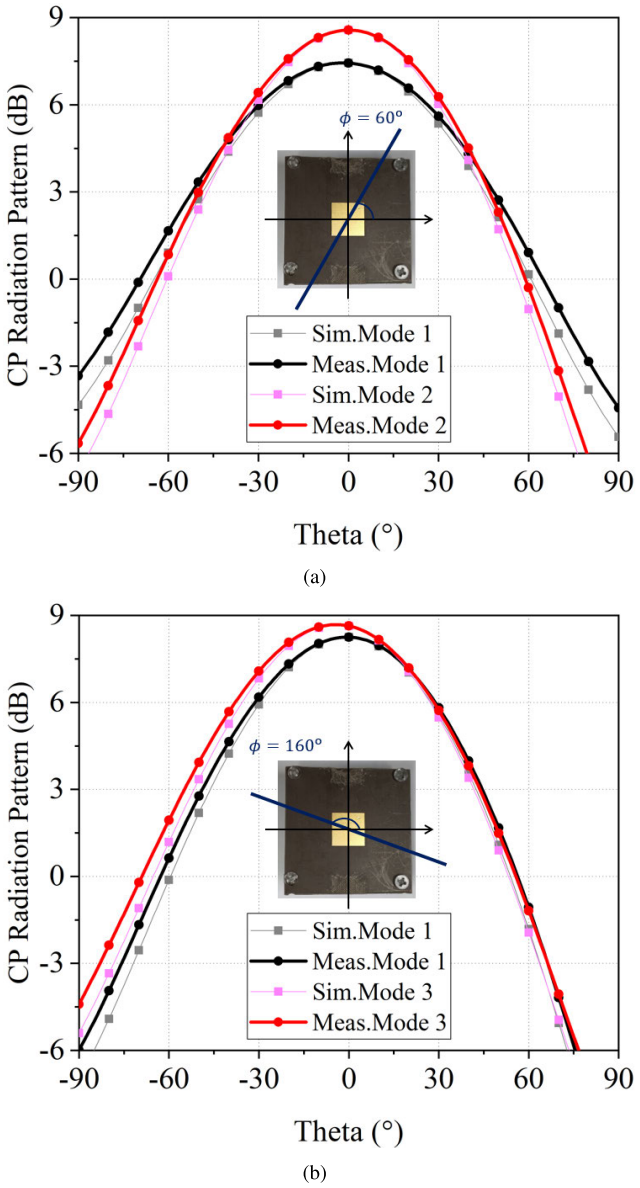


**FIGURE 11.** Measured CP radiation pattern: (a) $\phi = 60°$, (b) $\phi = 160°$.

performance. Also, the antenna has a low profile structure, which is suitable for mobile communication.

## IV. CONCLUSION

In this paper, a wideband circularly polarized antenna with a reconfigurable 2-dimensional axial ratio has been proposed. For mobile communication applications, a low-profile CP antenna is necessary. However, conventional CP antennas have a limited axial ratio bandwidth and scanning region. The reason for the low axial ratio is the amplitude difference ($\alpha$) and phase difference ($\Delta\Phi$) of the TM10 and TM01 signals. By controlling the amplitude and phase of the TM10 and TM01 signals, respectively, the axial ratio in a 2-dimensional region in a wide frequency bandwidth can be controlled. In the simulation, the axial ratio of the wideband CP antenna with the axial ratio controller was below 3 dB in the 2-dimensional region from −60° to 60° with a 20% fractional frequency bandwidth. Also, the wideband CP antenna with an axial ratio controller was implemented for verification. In the experiment, the proposed antenna had an axial ratio under 3 dB in the 2-dimensional region from −60° to 60° in the 20% fractional frequency bandwidth.

## REFERENCES

[1] K. L. Chung, X. Yan, Y. Li, and Y. Li, "A jia-shaped artistic patch antenna for dual-band circular polarization," *AEU Int. J. Electron. Commun.*, vol. 120, Jun. 2020, Art. no. 153207.
[2] B. Feng, Y. Tu, J. Chen, K. L. Chung, and S. Sun, "High-performance dual circularly-polarized antenna arrays using 3D printing for 5G millimetre-wave communications," *AEU Int. J. Electron. Commun.*, vol. 130, Feb. 2021, Art. no. 153569.
[3] B. Feng, L. Li, K. L. Chung, and Y. Li, "Wideband widebeam dual circularly polarized magnetoelectric dipole antenna/array with meta-columns loading for 5G and beyond," *IEEE Trans. Antennas Propag.*, vol. 69, no. 1, pp. 219–228, Jan. 2021.
[4] K. L. Chung, S. Xie, Y. Li, R. Liu, S. Ji, and C. Zhang, "A circular-polarization reconfigurable Meng-shaped patch antenna," *IEEE Access*, vol. 6, pp. 51419–51428, 2018.
[5] S. Gao, H. Lin, L. Ge, and D. Zhang, "A magneto-electric dipole antenna with switchable circular polarization," *IEEE Access*, vol. 7, pp. 40013–40018, 2019.
[6] P. Kumar, S. Dwari, R. K. Saini, and M. K. Mandal, "Dual-band dual-sense polarization reconfigurable circularly polarized antenna," *IEEE Antennas Wireless Propag. Lett.*, vol. 18, no. 1, pp. 64–68, Jan. 2019.
[7] M. Li, Y. Wu, W. Wang, and A. A. Kishk, "Wideband polarization reconfigurable differential circularly polarized antenna," *IEEE Access*, vol. 7, pp. 64697–64703, 2019.
[8] R. Xu, S. S. Gao, J. Li, K. Wei, and Q. Luo, "A reconfigurable dual-band dual-circularly polarized antenna for vehicle global navigation satellite system application," *IEEE Trans. Veh. Technol.*, vol. 69, no. 10, pp. 11857–11867, Oct. 2020.
[9] S. Wang, D. Yang, W. Geyi, C. Zhao, and G. Ding, "Polarization-reconfigurable antenna using combination of circular polarized modes," *IEEE Access*, vol. 9, pp. 45622–45631, 2021.
[10] W. Lin, S.-L. Chen, R. W. Ziolkowski, and Y. J. Guo, "Reconfigurable, wideband, low-profile, circularly polarized antenna and array enabled by an artificial magnetic conductor ground," *IEEE Trans. Antennas Propag.*, vol. 66, no. 3, pp. 1564–1569, Mar. 2018.
[11] M. Li, B. Xue, L. Li, Y. Xu, and Y. Guo, "A high-gain circular polarized microstrip slot coupling antenna for satellite communication," in *Proc. 6th Asia–Pacific Conf. Antennas Propag. (APCAP)*, Oct. 2017, pp. 1–3.
[12] S. Mener, R. Gillard, and L. Roy, "A dual-band dual-circular-polarization antenna for Ka-band satellite communications," *IEEE Antennas Wireless Propag. Lett.*, vol. 16, pp. 274–277, 2017.
[13] A. Catalani, G. Toso, P. Angeletti, M. Albertini, and P. Russo, "Development of enabling technologies for Ku-band airborne SATCOM phased-arrays," *Electronics*, vol. 9, no. 3, p. 488, Mar. 2020.
[14] C. Wang, F. Zhang, F. Zhang, Y.-L. Yao, and T. Li, "Compact wide-beam circularly polarized antenna with stepped Arc-shaped Arms for CNSS application," *Prog. Electromagn. Res. C*, vol. 71, pp. 141–148, 2017.
[15] X. Zhang, L. Zhu, and N.-W. Liu, "Pin-loaded circularly-polarized patch antennas with wide 3-dB axial ratio beamwidth," *IEEE Trans. Antennas Propag.*, vol. 65, no. 2, pp. 521–528, Feb. 2017.
[16] H. Liu, C. Xun, S.-J. Fang, and Z. Wang, "Compact dual-band circularly polarized patch antenna with wide 3-dB axial ratio beamwidth for BeiDou applications," *Prog. Electromagn. Res. M*, vol. 87, pp. 103–113, 2019.
[17] Z.-P. Zhong, X. Zhang, J.-J. Liang, C.-Z. Han, M.-L. Fan, G.-L. Huang, W. Xu, and T. Yuan, "A compact dual-band circularly polarized antenna with wide axial-ratio beamwidth for vehicle GPS satellite navigation application," *IEEE Trans. Veh. Technol.*, vol. 68, no. 9, pp. 8683–8692, Sep. 2019.
[18] S. Liu, D. Yang, and J. Pan, "A low-profile circularly polarized metasurface antenna with wide axial-ratio beamwidth," *IEEE Antennas Wireless Propag. Lett.*, vol. 18, no. 7, pp. 1438–1442, Jul. 2019.
[19] C. Li, F.-S. Zhang, F. Zhang, and K. Yang, "A wideband circularly polarized antenna with wide beamwidth for GNSS applications," *Prog. Electromagn. Res. C*, vol. 84, pp. 189–200, 2018.

[20] L. Zhang, S. Gao, Q. Luo, P. R. Young, W. Li, and Q. Li, "Inverted-S antenna with wideband circular polarization and wide axial ratio beamwidth," *IEEE Trans. Antennas Propag.*, vol. 65, no. 4, pp. 1740–1748, Apr. 2017.
[21] R. Galuscak and P. Hazdra, "Circular polarization and polarization losses," in *Proc. DUBUS*, 2006, pp. 8–23.

**JEONG-WOOK KIM** received the B.S. degree in electronics engineering from Pusan National University (PNU), Busan, South Korea, in 2018, and the M.S. degree in electronics and electrical engineering from the Korea Advanced Institute of Science and Technology (KAIST), in 2020, where he is currently pursuing the Ph.D. degree in electronics and electrical engineering.

His current research interests include active phased array antenna systems, wireless power charging systems, invisible antenna, RADAR systems, and signal processing.

**JU-IK OH** received the B.S. degree in electronic engineering from Inha University, Incheon, Republic of Korea, in 2017, and the M.S. degree in electrical engineering from the Korea Advanced Institute of Science and Technology (KAIST), Daejeon, Republic of Korea, in 2019, where he is currently pursuing the Ph.D. degree in electrical engineering.

His current research interests include millimeter-wave antennas, RF front-end design, and antenna array systems.

**SANG HYUCK HAN** received the B.S. and M.S. degrees in electrical and electronic engineering from Yonsei University, Seoul, South Korea, in 2018 and 2020, respectively. He is currently pursuing the Ph.D. degree in electrical engineering with the Korea Advanced Institute of Science and Technology (KAIST), Daejeon, South Korea.

His research interests include RF systems, phased array systems, antenna design, and bio-signal sensing.

**WON-YOUNG SONG** was born in Daejeon, South Korea, in 1986. He received the B.S. and Ph.D. degrees in electrical engineering from the Korea Advanced Institute of Science and Technology (KAIST), Daejeon, in 2008 and 2020, respectively. He is currently working as a Senior Researcher with the Electronics and Telecommunications Research Institute (ETRI).

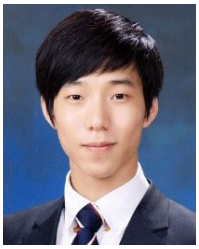

**SOO-CHANG CHAE** received the B.S., M.S., and Ph.D. degrees in electrical engineering from the Korea Advanced Institute of Science and Technology (KAIST), Daejeon, South Korea, in 2014, 2016, and 2021, respectively. He is currently working as a Senior Researcher with Samsung Electronics. His current research interests include near-field wireless charging systems, antenna design, RF/microwave circuit design, and active phased array antenna systems.

**JONG-WON YU** (Member, IEEE) received the B.S., M.S., and Ph.D. degrees in electrical engineering from the Korea Advanced Institute of Science and Technology (KAIST), Daejeon, South Korea, in 1992, 1994, and 1998, respectively.

From 1995 to 2000, he was with Samsung Electronics, Suwon, South Korea. From 2000 to 2001, he was with Wide Telecom, Seoul, South Korea. From 2001 to 2004, he was with Telson Electronics, Seoul. In 2004, he joined KAIST, as an Assistant Professor, where he is currently a Professor with the School of Electrical Engineering. His current research interests include microwave/millimeter-wave circuit (hybrid), wireless power transfer, wireless/near-field communication systems, and radio frequency identification/ubiquitous sensor networks (USNs).